Direct measurement of the $\bar{K}N \to \pi\Sigma$ scattering amplitude below the $\bar{K}N$ threshold employing the $d(K^-, N)$"$\pi\Sigma$" reaction

Kentaro Inoue

October 30, 2022

Contents

Chapter 1

Discussion

1.1 $\pi\Sigma$ spectra

In this section, we first describe how to classify the $\pi\Sigma$ modes and convert the spectra obtained from MC simulations with acceptance correction to cross sections. For forward protons, the solid angle of the forward proton detector depends on the momentum due to the beam-swept magnet. This effect is also evaluated using MC simulations.

1.1.1 Mode decomposition of $d(K^-, p)$

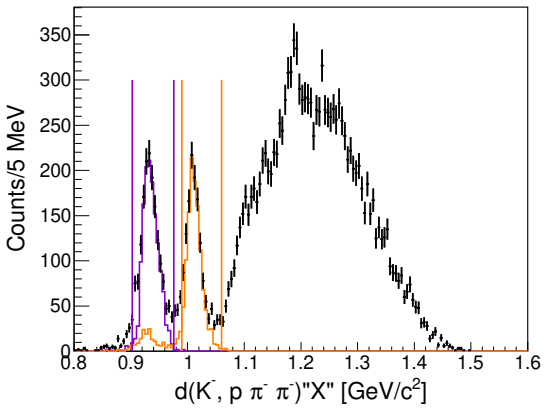

Figure 1.1: This figure shows the missing mass of $d(K^-, p\pi^-\pi^-)$. Orange and purple lines indicate selection region as missing p and $p\pi^-$, respectively. $d(K^-, p\pi^-)$"Σ^0" and $d(K^-, p\pi^-)$"Λ" tagged events are drawn orange and purple plot in same figure.

In the case of forward protons, the $\pi^-\Sigma^0$ mode is identified from the event where two π^- are detected by the CDS. The $\pi^-\Sigma^0$ mode has the

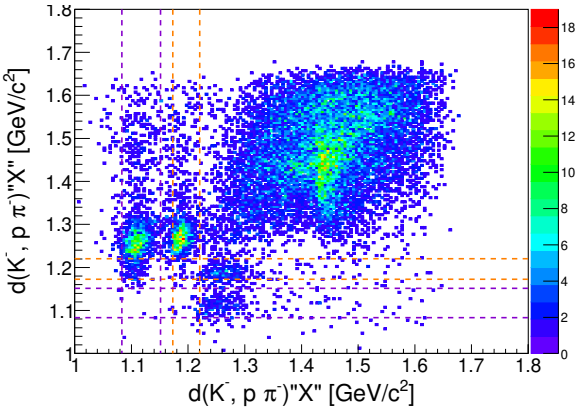

Figure 1.2: This figure shows the scatter plot of the $d(K^-, p\pi^-)$ missing masses in the p and two π^- detected events. Horizontal axis represents nearer DCA π^- and virtical axis represents other one. Orange and purple lines indicate selection region as $d(K^-, p\pi^-)$"Σ^0" and $d(K^-, p\pi^-)$"Λ", respectively.

following decay chain.

$$K^- d \to p\pi^- \Sigma^0 \to p\pi^- \Lambda\gamma \to p\pi^- \gamma p\pi^-$$

And $\pi^-\Lambda$ mode has a similar decay chain.

$$K^- d \to p\pi^- \Lambda \to p\pi^- p\pi^-$$

We identify the $\pi^-\Sigma^0$ mode by identifying Σ^0 with $d(K^-, p\pi^-)$ missing mass and $p\gamma$ with $d(K^-, p\pi^-\pi^-)$ missing mass.

The $d(K^-, p\pi^-\pi^-)$ missing mass is plotted in the Figure.**??**, with the Σ^0 identified from the $d(K^-, n\pi^-)$ missing mass as the orange histogram and the Λ identified as the purple histogram. In this reaction, $p\gamma$ make a peak like structure as this figure, because $\pi^-\Sigma^0$ momentum is small and γ momentum is restricted. Therefore, not only the $\pi^-\Lambda$ Λ mode missin p but also the $\pi^-\Sigma^0$ missing $p\gamma$ can be identified, the range for each identification is represented by the purple and orange vertical lines.

1.1.2 Mode decomposition of $d(K^-, n)$

In the case of forward neutrons, the missing neutron is identified from the $d(K^-, n\pi^-\pi^+)$ missing mass as shown in the Figure.1.3, and the $K^- d \to n\pi^-\pi^+$"n" final state is identified. The following reactions are possible for this final state.

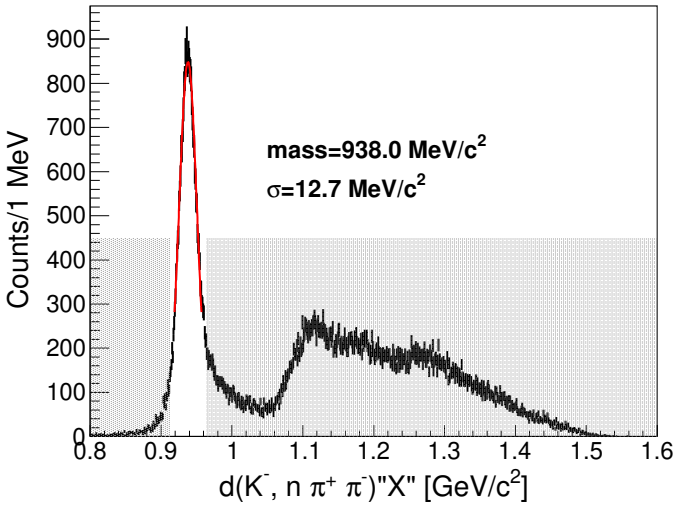

Figure 1.3: This figure shows $d(K^-, n\pi^+\pi^-)"X"$ spectrum. Red line indicates fittig gaussian and gray hatched region indicates rejected region for $d(K^-, n\pi^+\pi^-)"n"$ events.

$$K^- d \to K^0 nn \tag{1.1}$$
$$K^- d \to \Sigma^+_{froward} \pi^- n \tag{1.2}$$
$$K^- d \to \Sigma^-_{froward} \pi^+ n \tag{1.3}$$
$$K^- d \to \Sigma^+ \pi^- n_{forward} \tag{1.4}$$
$$K^- d \to \Sigma^- \pi^+ n_{forward} \tag{1.5}$$

In the reaction.(1.1) of these reactions, K^0 is produced and K0 decays to π^+ and π^+. And the reacion.(**??**) and reaction.(**??**) produce forward charged Σ. The neutrons measured by the forward detector are decays from the produced Σ.

These three reactions can be identified by reconstructing K^0 from the invariant mass of π^+ and π^-, Σ^+ from neutron and π^++, and Σ^- from neutron and π^-, as shown in the Figure.**??**.

The remaining reactions.(1.4) and (1.5) are 2-step reactions in which the $\bar{K}$ meson kicks the neutron forward and reacts with the residual nucleon, scattering $\pi\Sigma$ backward, which is the signal we want to measure.

The two modes are identified by the $d(K^-, n\pi)$ missing masses as shown in Figure.**??**. In that figure for example, in the case of the $\pi^-\Sigma^+$ mode,

the missing mass of the charge opposite to Σ results in the correct Σ peak as shown in the red line, while the missing mass of π decays from Σ and is widely distributed in the kinematically allowed region without any structure as shown in the blue line.

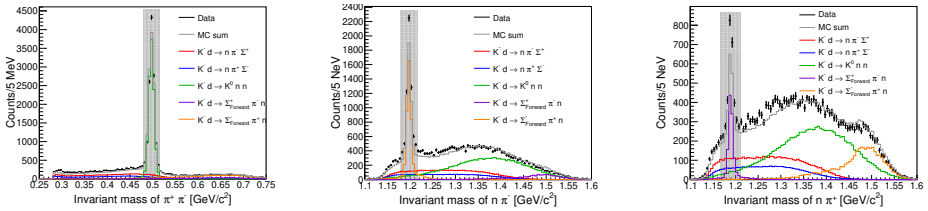

Figure 1.4: These figures shows invariant masses of $\pi^+\pi^-$, $n\pi^-$ and $n\pi^+$ with fitting result of 5 reactions.

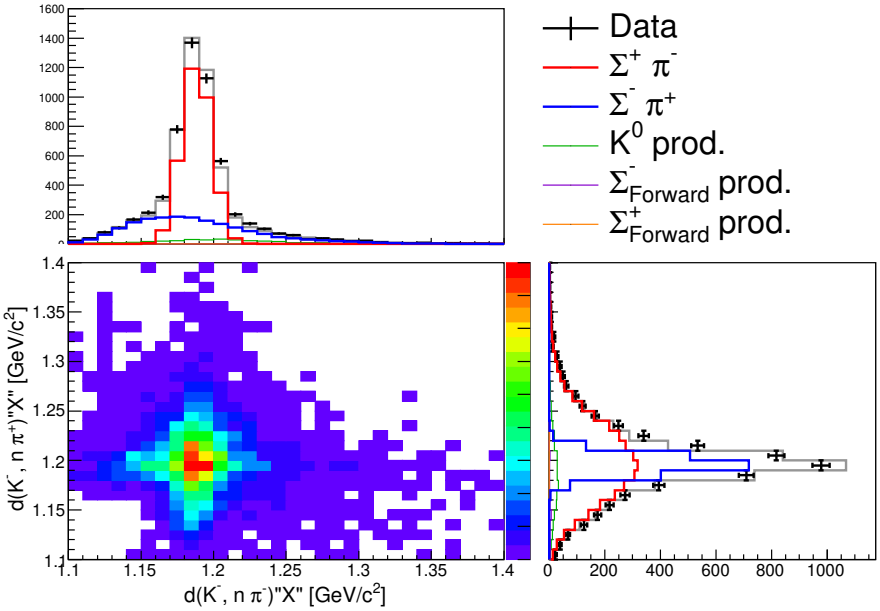

Figure 1.5: This figure indicates summed up fitting result and log-likelihood value of each bins.

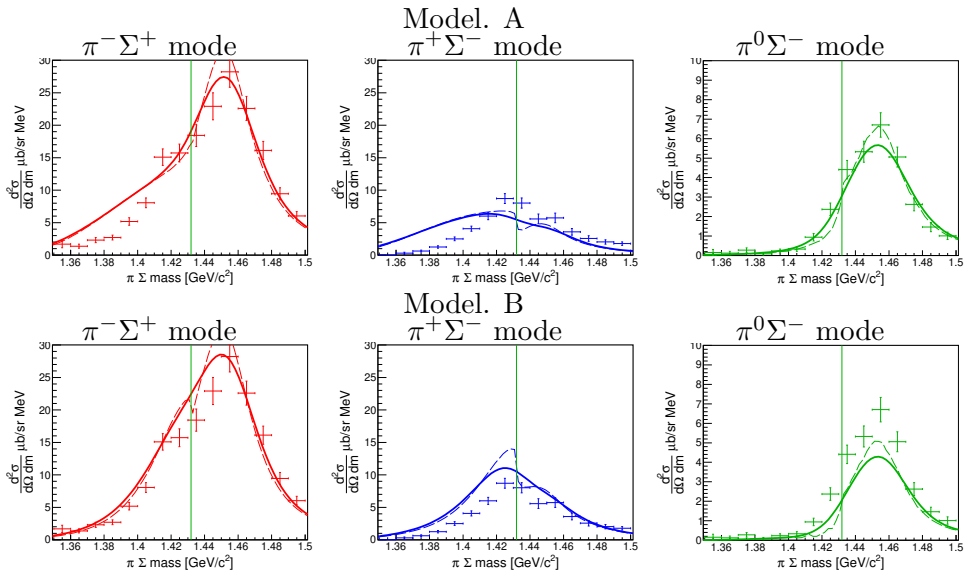

Figure 1.6: This figures shows obtained spectra and DCC calculation [44]. Error bar indicates obtained spectra. Dashed and solid line indicate theoretical calculation itself and calculation convoluted by detector resolution, respectively. Left, center and right figures represent $\pi^-\Sigma^+$, $\pi^+\Sigma^-$and $\pi^0\Sigma^-$, respectively.

1.2 Comparison with DCC model

The DCC model [**?**] is constructed from fitting of various $K^-p \to$ meson-baryon data from the $\bar{K}N$ threshold to $W = 2.1GeV/c$ as described in section, the model can treat comprehensively scattering including strangeness in wide energy region which including high energy 1-step $K^-p \to \bar{K}N$ scattering and $\bar{K}N \to \pi\Sigma$ scattering below the $\bar{K}N$ threshold, however the region below the threshold is extrapolation. The theoretical calculation by the model was performed [44]. We ploted into same figure as shown in Fig1.6. The obtained data was plotted as error bars and theoretical calculation was plotted as lines. The dashed line indicates theoretical calculation itself and the solid line indicates them convoluted by the detector resolution which shown in Fig.B.4. The overall strength of each spectra is well matched, which means this reaction mechanism seems to consider 2-step reaction of $K^-N \to \bar{K}N$ and $\bar{K}N \to \pi\Sigma$ is dominant as described in Sec.**??**.

Next, we comparison with decomposed component of $I = 1$, $I = 1$ and these interference term as shown in Fig.1.7 to discuss about detail spectra shape. While interference term seems to be well matched each models, there are some difference about $I = 0$ and $I = 1$, which is different part of each spectra depend on the model. In the case of $I = 0$ channel, model.A differ about the spectrum shape. On the other hand, model.B seems to be better

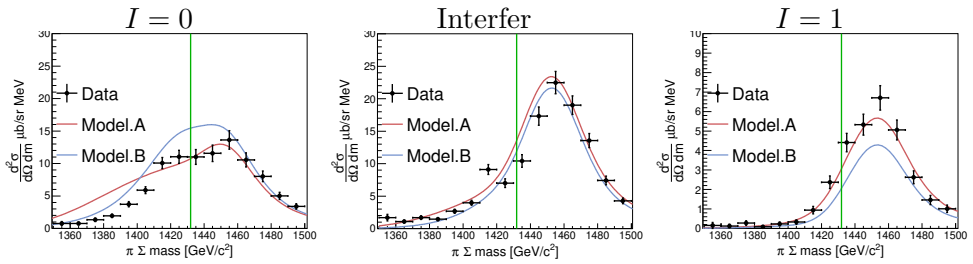

Figure 1.7: These figures show comparison with decomposed $I = 0$, $I = 1$ and these interference term. Left, center and right represent about $I = 0$, interference and $I = 1$ component, respectively. Dark red and dark blue indicate model.A and model.B, respectively.

matched than model.A. The fact is considered due to large width of higher mass region pole on model.A, so model.A has a long tail component below the $\bar{K}N$ threshold, which component can not be explain the data. Model.B is good matched about spectrum shape, but the strength of theoretical calculation is shortage.

1.3 Demonstration of fitting by DCC models

Next, we performed demonstration of fitting by DCC models to discuss each component how to contribute each spectra. First, we use the strength of $I = 0$ and $I = 1$ as free parameter, which scale $I = 0$ and $I = 1$ spectra. The interferance term also change corespond to the isospin relation as follow rrepresentation.

$$\begin{aligned}
\frac{d\sigma_{\pi^-\Sigma^+}}{dMd\Omega} &= \frac{1}{3}A_{I=0}|T_{I=0}|^2 + \frac{1}{2}A_{I=1}|T_{I=1}|^2 + \frac{2}{\sqrt{6}}\sqrt{A_{I=0}A_{I=1}}\mathbf{Re}(T_{I=0}T^*_{I=1}) \\
\frac{d\sigma_{\pi^+\Sigma^-}}{dMd\Omega} &= \frac{1}{3}A_{I=0}|T_{I=0}|^2 + \frac{1}{2}A_{I=1}|T_{I=1}|^2 - \frac{2}{\sqrt{6}}\sqrt{A_{I=0}A_{I=1}}\mathbf{Re}(T_{I=0}T^*_{I=1}) \\
\frac{d\sigma_{\pi^0\Sigma^-}}{dMd\Omega} &= \frac{1}{2}A_{I=1}|T_{I=1}|^2
\end{aligned} \tag{1.6}$$

Where, $A_{I=0}$ and $A_{I=1}$ is scaling factor introduced as 2-step scattering strength. And interference term is changed according to square root of each strength.

Fig.[1.8] shows about fitting result of Model.A, in which above figures show obtained spectra and bottom figures show calculated spectra. We note that fitting are used only above 3 spectra. At the result, we obtain $A_{I=0} = 0.562 \pm 0.015$ and $A_{I=1} = 1.070 \pm 0.040$ with $\chi^2/NDF = 691/42 \sim 16.4$. In the model.A, $\pi^-\Sigma^0$ of $I = 1$ is obtained good matched, that strongly affect

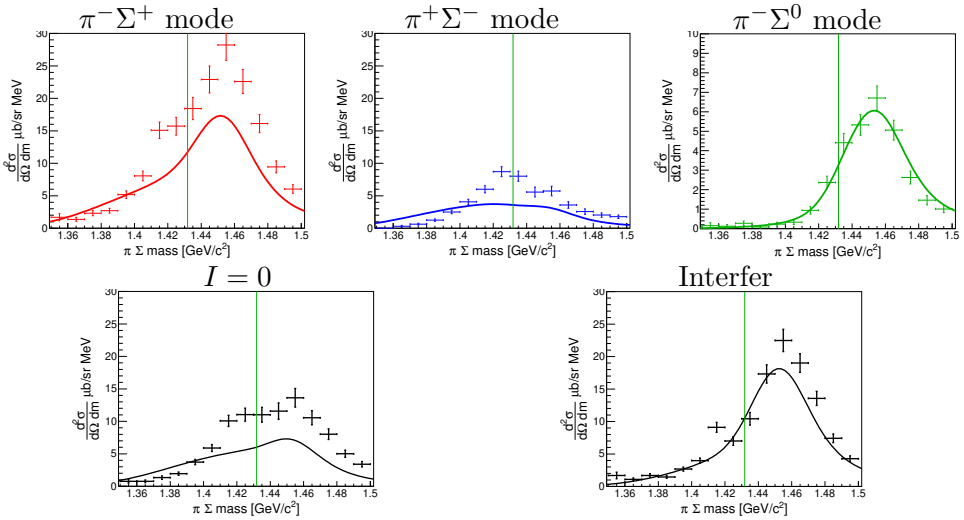

Figure 1.8: These figures show fitting result about $A_{I=0}$ and $A_{I=1}$ using model.A. Above figures are used fitting. Left, center and right represents $\pi^-\Sigma^+$, $\pi^+\Sigma^-$ and pure $I = 1$ $\pi^-\Sigma^0$ channels. Bottom figures show calculated components. Left and right indicate $I = 0$ and $I = 0$ and $I = 1$ interference. (Pure $I = 1$ corespond to $\pi^-\Sigma^0$(top right))

above the threshold, but I=0 below the threshold is not matched. Therefore, the model.A can not explained obtained spectra, as the shown Fig.[1.8].

On the other hand, the result of the model.B is shown as the Fig.[1.9], and the parameters are obtained at $A_{I=0} = 0.721 \pm 0.016$ and $A_{I=1} = 1.423 \pm 0.055$ with $\chi^2/NDF = 220/42 \sim 5.25$. In the model.B, $I = 1$ strength is recovered and overall each spectra shape are matched. But, theoretical strength of $\pi^+\Sigma^-$ is shortage above the $\bar{K}N$ threshold. That appears in $I = 0$ spectra.

Next, we introduce scaling factor B about interference term to study how to improve fitting and how interference term work. Then, $\pi^-\Sigma^+$and $\pi^+\Sigma^-$cross section represents as follow.

$$\begin{aligned}\frac{d\sigma_{\pi^-\Sigma^+}}{dMd\Omega} &= \frac{1}{3}A_{I=0}|T_{I=0}|^2 + \frac{1}{2}A_{I=1}|T_{I=1}|^2 + \frac{2}{\sqrt{6}}B\sqrt{A_{I=0}A_{I=1}}\mathbf{Re}(T_{I=0}T^*_{I=1}) \\ \frac{d\sigma_{\pi^+\Sigma^-}}{dMd\Omega} &= \frac{1}{3}A_{I=0}|T_{I=0}|^2 + \frac{1}{2}A_{I=1}|T_{I=1}|^2 - \frac{2}{\sqrt{6}}B\sqrt{A_{I=0}A_{I=1}}\mathbf{Re}(T_{I=0}T^*_{I=1})\end{aligned} \tag{1.7}$$

Because $\pi^-\Sigma^0$ is pure $I = 1$ channel, we performed fitting $I = 1$ channel is determined from only $\pi^-\Sigma^0$, then $I = 0$ and the interference term decided, whose result is shown in Fig.[1.10]. The $\chi^2/NDF = 187/41 \sim 4.56$ is improved than 5.25 of Fig.[1.9]. Parameters are $A_{I=0} = 0.686 \pm 0.017$, $A_{I=1} = 1.462 \pm 0.059$ and $B = 0.828 \pm 0.030$ in this fitting.

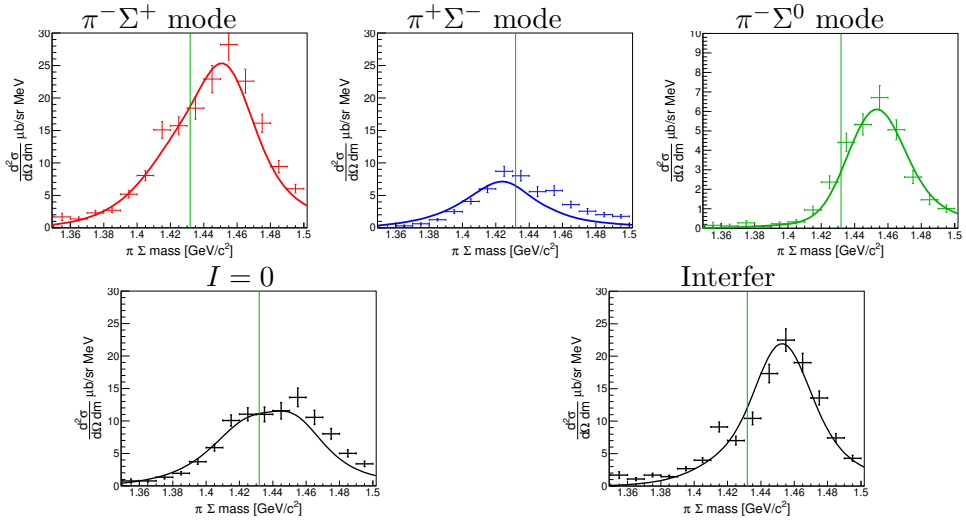

Figure 1.9: These figures show fitting result about $A_{I=0}$ and $A_{I=1}$ using model.B with same notation of Fig[1.8].

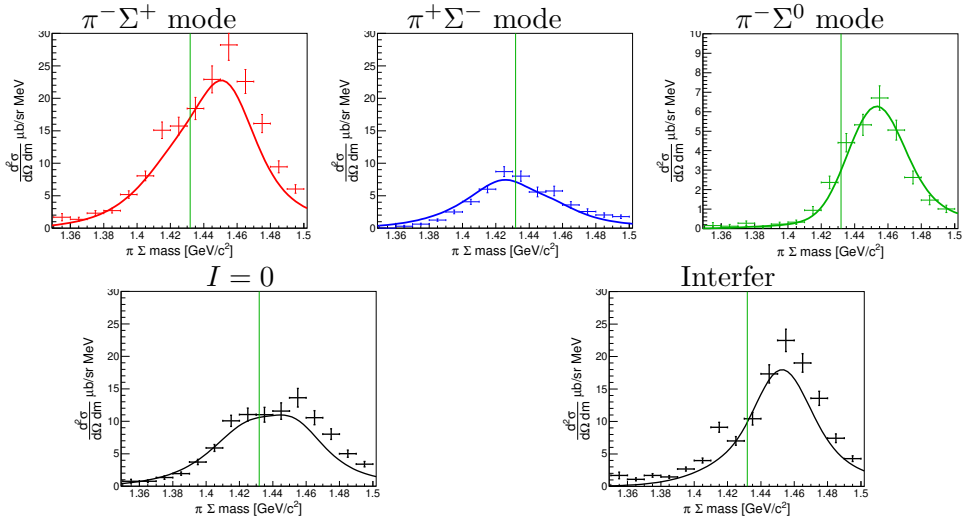

Figure 1.10: These figures shows result of the fitting, in which $I = 1$ is decided by $\pi^-\Sigma^0$ and $I = 0$ and interference term are determined after. The figure notation is same as Fig.[1.8].

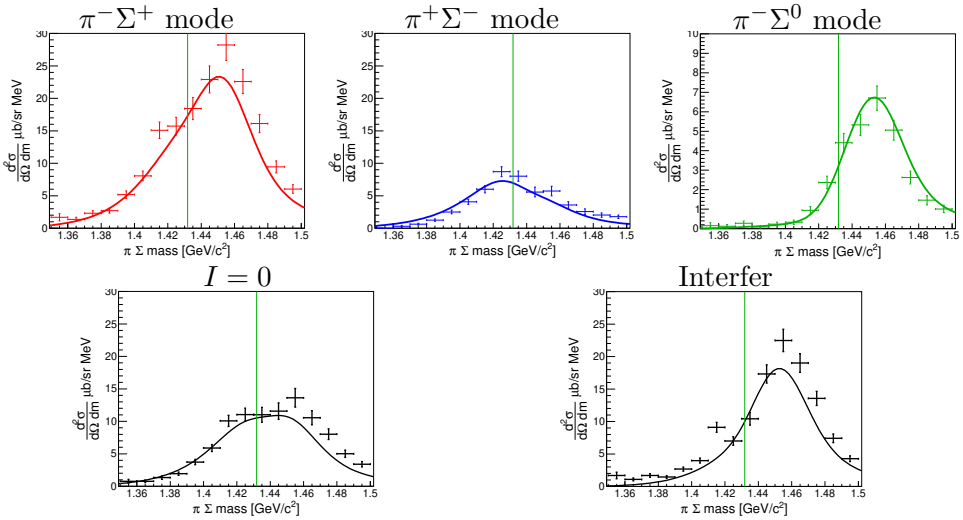

Figure 1.11: These figures show fitting result about $A_{I=0}$, $A_{I=1}$ and B that is the scaling factor about interference term using model.B with same notation of Fig[1.8].

The case of simultaneous fitting of these three parameters is shown in the Fig.[1.11], whose $\chi^2/NDF = 184/41 \sim 4.48$ is almost same at 4.56 of the case of $I = 1$ separately decided. Then, parameters is $A_{I=0} = 0.682 \pm 0.017$, $A_{I=1} = 1.570 \pm 0.058$ and $B = 0.811 \pm 0.030$.

Table.[**??**] lists fit parameters using the DCC model. $I = 0$ component is scaled down to 72% and $I = 1$ component is scaled up to 142% at fitting using $I = 0$ and $I = 1$ scale factor. Then the interference factor is added, the factor of $I = 0$ component is a bit descried and become to 68%, and the factor of $I = 1$ component is increased and change to $146 - 156\%$. The interference term is descried to $83 - 81\%$.

Chapter 2

Conclusion

We measured $d(K^-,N)"\pi\Sigma"$ reaction with $1GeV/c$ K^- beam at K1.8BR beamline of the hadron hoall in the J-PARC as the J-PARC E31 experiment. We measured forward scattering scattering nucleon using the NC and PC. Simultaneously, decayed particles are detected by the CDS surrounding the liquid-D_2 target to identified final state. We identify $K^-d \to n\pi^+\pi^-n$ final state and removed K^0 and forward-$\Sigma^\pm$ production, in which forward-$\Sigma^\pm$ means forward neutron decayed from $\Sigma^\pm$. And, we obtain $d(K^-,n)"\pi^\mp\Sigma^\pm"$, which decomposed to $\pi^-\Sigma^+$ and $\pi^+\Sigma^-$ from missing mass of $d(K^-,n\pi^\mp)"\Sigma^\pm"$. We identify $\pi^-\Sigma^0$ final state from identify $d(K^-,p\pi^-)"\Sigma^0"$ and $d(K^-,p\pi^-\pi^-)"p"$. At the result, We obtained $\pi^-\Sigma^+$, $\pi^+\Sigma^-$and $\pi^0\Sigma^-$cross sections from the missing mass of the $d(K^-,N)$ missing mass.

This reaction is considered as the 2-step reaction of $K^-N \to \bar{K}N$ scattering and $\bar{K}N \to \pi\Sigma$ scattering. 1-step reaction has large energy $\sim 2.05GeV/c$ and 2-step can allow to occur $\bar{K}N \to \pi\Sigma$ below the $\bar{K}N$ threshold. Large energy 1-step reaction restricts the contamination from 1-step reaction in which a nucleon emitted as the spectator around the $\bar{K}N$ threshold. Because the recoiled $\bar{K}$ has low momentum $\sim 0.25GeV/c$ around the $\bar{K}N$ threshold, the S-wave scattering is dominant in 2-step $\bar{K}N \to \pi\Sigma$ scattering, which is confirmed from our data not to see obvious peak around the $\Sigma(1385)$ and $\Lambda(1520)$, which are P-wave and D-wave. We can understand the reaction is the above the mechanism from the matching our data and theoretical calculations which adopts or covers around high energy $\bar{K}N$ scattering region around 1-step.

We decompose about the isospin $I = 0$, $I = 1$ and these interference term about 2-step scattering. The so-called model.B is not matched spectra shape of $\pi^-\Sigma^+$ and $\pi^+\Sigma^-$, especially below the $\bar{K}N$ threshold, because this has large width of higher pole. On the other hand, in model.B, obtained spectra are reproduced to change all $I = 0$, $I = 1$ and these interference term. That means that $I = 0$ component is important, but $I = 1$ component is also important even though the component does not have pole in the region

of interest. That means that $I = 0$ component is important, but $I = 1$ component is also important even though the component does not have pole in the region of interest. Above the threshold, $I = 0$ $\pi^-\Sigma^0$ has large cross section and the interference term between $I = 0$ and $I = 1$ also appear as the difference of $\pi^-\Sigma^+$ and $\pi^+\Sigma^-$. So, interference term is necessary to explain the these three spectra.

We obtain $\pi^-\Sigma^+$, $\pi^+\Sigma^-$ and $\pi^-\Sigma^0$ spectra via the $d(K^-, N)$ reaction, which is considered 2-step reaction of $K^-N \to \bar{K}N$ and $\bar{K}N \to \pi\Sigma$. These spectra provide all information to determine that $I = 0$, $I = 1$ and these interference term of $\bar{K}N \to \pi\Sigma$ scattering around the $\bar{K}N$ threshold.

Appendix A

Offline selection

Decayed particles sometimes make fake trajectories and hits in the CDC and the CDH. For expamle, neutral particles convert to charged particles at the solenoid magnets and these make hit in the CDH. We select event by simple offline analysis to avoid these fake hits.

A.1 $d(K^-, n\pi^+\pi^-)$

FigA.1 shows scatter plot of T0-CDH tof and energy deposit of the CDH by $\pi^+\pi^-$ in $n_{forward}$ and $\pi^+\pi^-$ detected events. There are some events in slow region and low energy deposit region which will be fake events from low energy electron and decayed muon and so on. We select time window of 1–15 [ns] to reject these fake hits. FigA.2 shows energy deposit of $\pi^+\pi^-$ in smae events. Red lines indicates energy deposit summed up clustering hits. So, low energy deposit includes events that a pion pass through edge of the CDH. We select two CDH clusters event accociating CDC tracks after hits filtered by time-window for $d(K^-, n\pi^+\pi^-)$ events. We also select energy deposit of the cluster more than 4.5 $[MeVee]$.

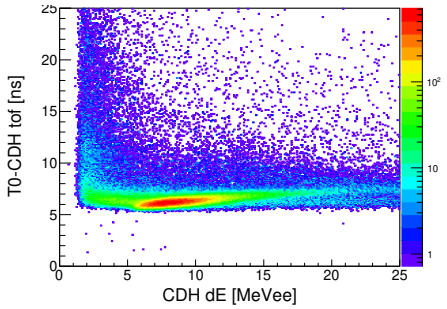

Figure A.1: The figure indicates T0-CDH tof and energy deposit of the CDH of $\pi^+\pi^-$ hits in $d(K^-, n\pi^+\pi^-)$ events

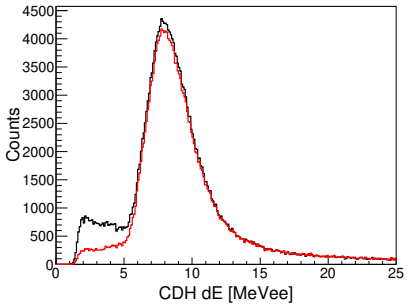

Figure A.2: This figure shows $\pi^+\pi^-$ energy deposit of the CDH in same condition of FitA.1. Black line indicate no selection and red line indicate clustering energy deposit.

A.2 $d(K^-, p\pi^-\pi^-)$

$d(K^-, p\pi^-\pi^-)$ event selection is same as $d(K^-, n\pi^+\pi^-)$ event. So, CDH hits were adopted timewindow and clustering as same as $d(K^-, n\pi^+\pi^-)$ analysis which was shown in FigA.3

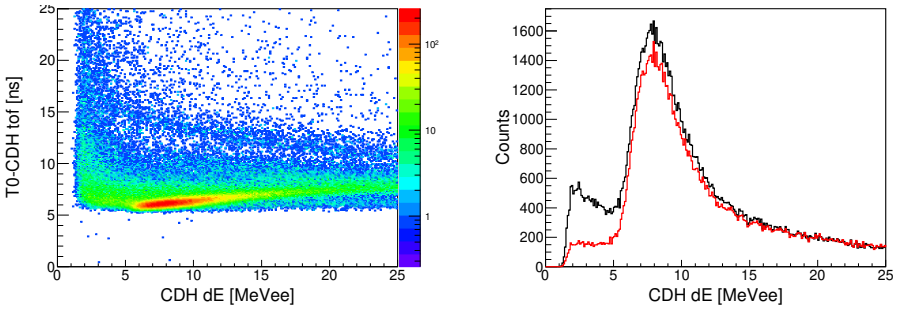

Figure A.3: These figures represent about offline selection for $d(K^-, p\pi^-\pi^-)$ events. Left figure shows scatter plot of T0-CDH tof and CDH dE in forward proton and 2 π^- detected events. Right figure shows CDH dE in which black line indicates without clustering and red line indicates with clustering.

Appendix B

Geant4 simulation

In this thesis, the Monte Carlo simulation was employed Geant4.10.01.p01 toolkit with the QGSP_BERT_HP physics package. This physics package adopts precompound model for high energy hadrons ($10 - 25GeV/c$)which are protons, neutrons, pions, kaons and nuclei and Bertini cascade for low energy hadrons ($\sim 10GeV/c$). HP means high precision for the neutron espacially thermal neutron ($< 20MeV/c$), so these neutrons were transported by the high precision data.

The purposes of Monte Carlo are evaluation of the acceptance of the CDS and estimation of contribution from specific reactions. 1-step reactions was simulated using previous experimental data of $\bar{K}N$ scattering and fermi momentum, which was used to evaluate contamination to 2-step reactions in this thesis. Also, 2-step reactions was simulated as S-wave scattering, which was used to evaluated the acceptance of the CDS. In $d(K^-, n\pi^+\pi^-)"n"$ final state, 2-step simulation of $d(K^-, n)"\pi^\mp\Sigma^\pm$ was used to separation of each modes by template fittings. As Sec**??**, this final state was sucessfully decomposed to 5 reactions which are $K^-d \to \pi^\mp\Sigma^\pm n$ (1-step), $K^-d \to K^0nn$ (1-step) and $K^-d \to n\pi^\mp\Sigma^\pm$ (2-step).

The result of the Monte Carlo simulation of $d(K^-, n\pi^+\pi^-)"n"$ final state and template fitting was used for some calibrations. The CDS magnetic field was calibrated using K^0 peak which was subtracted background which was shown in FigB.1. We searched correct field value value while changing the inputed field value that indicates in FigB.2. The CDC resolution was estimated at $280\mu m$ using width of K^0 peak while changing the inputed resolution.

The NC resolution was evaluated $d(K^-, n\pi^+\pi^-)"n"$ peak which was shown in FigB.4. The $K^-d \to n\pi + \pi^-n$ events was decomposed which described in Sec**??**, so red plot in FigB.4 was reproduced using the Monte Carlo samples and template fitting. The NC time resolution was estimated at $170ps$ while changing the inputed resolution for the Monte Carlo simulation. The PC/CVC time resolution is adopted similar procedure to

$d(K^-, p\pi^-\pi^-)"p"$ peak which is come from the $K^-d \to p\Lambda\pi^-$ scattering as shown in FigB.5.

The $d(K^-, n)"X"$ missing mass resolution was estimated using the $d(K^-, n)"\pi^{\mp}\Sigma^{\pm}"$ Monte Carlo simulation as shown in FigB.6, so we estimated about $10MeV/c^2$ at the $\bar{K}N$ threshold. The resolution was given 3rd polynomial function by fitting to this figure which was shown in same figure.

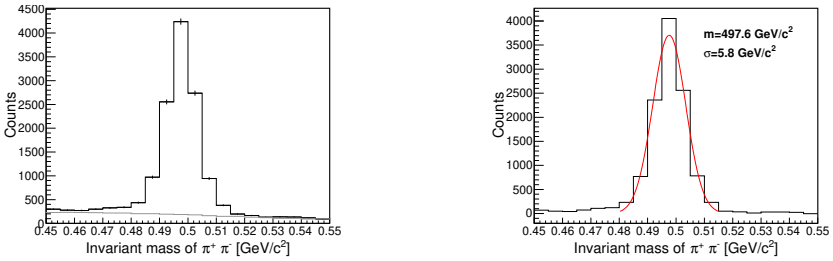

Figure B.1: Right figure shows the invariant mass of $\pi^+\pi^-$ in the $d(K^-, n\pi^+\pi^-)"n"$ missing masses with estimated background which was indicated as gray line. Left figure shows the K^0 peak which was subtracted spectrum with fitted Gaussian, that was red line.

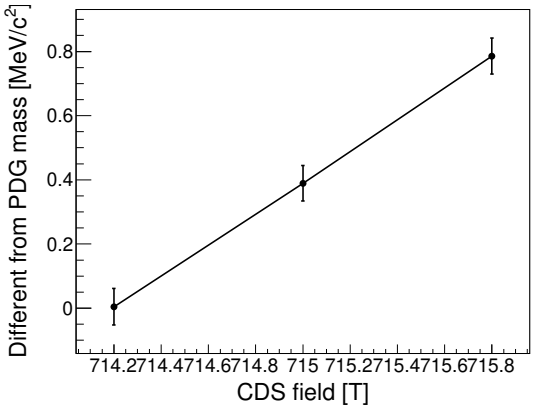

Figure B.2: This figure indicates relation of the CDS field value and K^0 peak position which was indicated in left figure of FigB.1.

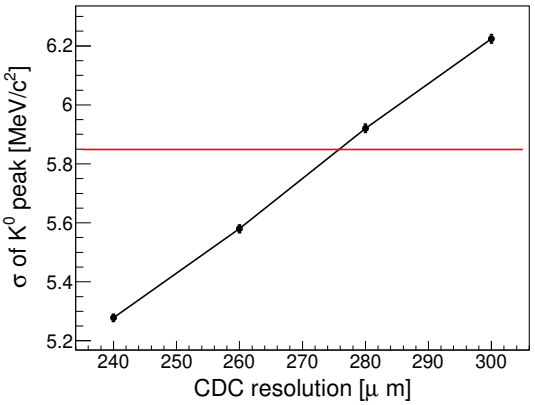

Figure B.3: This figure indicates relation of the CDC resolution and width of K^0 peak. Red line indicates width of K^0 peak by data which was discribed in left figure of FigB.1.

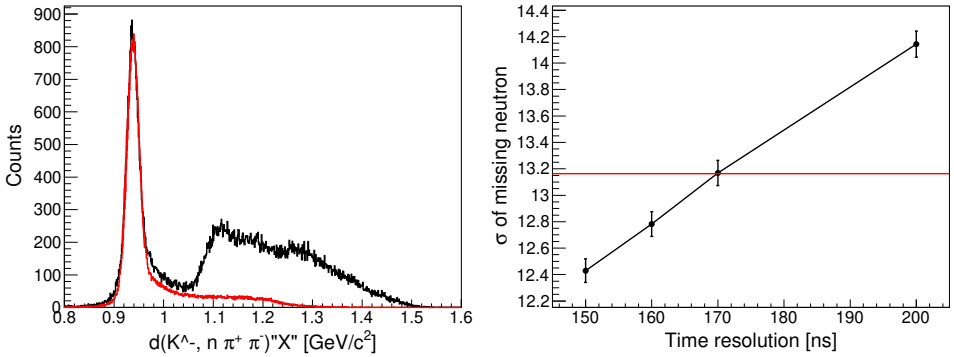

Figure B.4: Left figure shows $d(K^-, n\pi^+\pi^-)$"n" missing mass spectra. Black one indicates data and red one indicates the summed up Monte Carlo simulation datas. Right figure indicates relation of σ of $d(K^-, n\pi^+\pi^-)$"n" peak which was estimated Gaussian fitting and inputed time resolution. Red line indicate fitting result of the data.

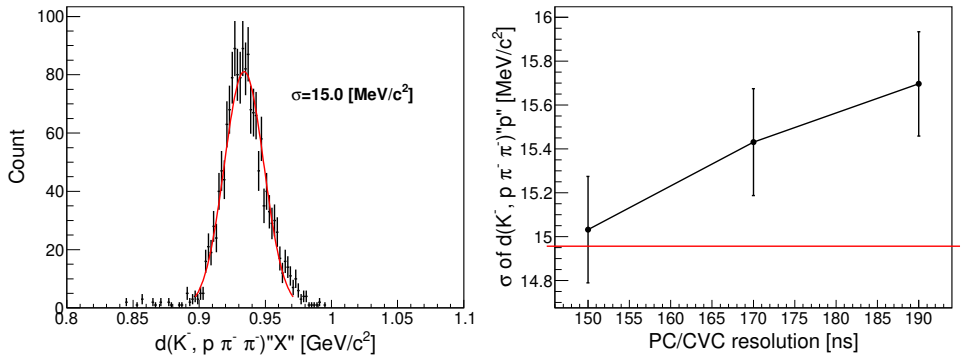

Figure B.5: Left figure shows $d(K^-, p\pi^-\pi^-)$"p" missing mass spectrum in $d(K^-, p)$"$\pi^-\Lambda$" events. Red line indicates fitting result. Right figure indicates relation of σ of $d(K^-, p\pi^-\pi^-)$"p" peak which was estimated Gaussian fitting and inputed time resolution. Red line indicate fitting result of the data.

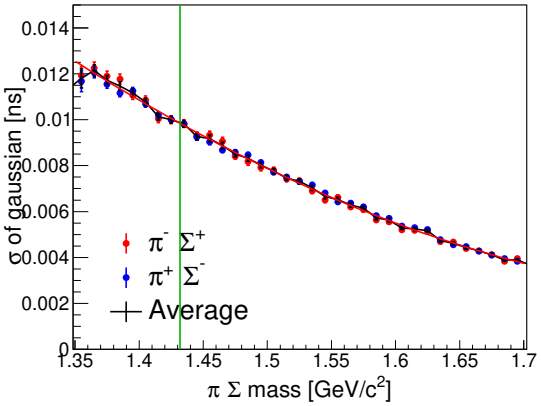

Figure B.6: This figure indicates about $d(K^-, n)$"X" missing mass resolution which was estimated by the $d(K^-, n)$"$\pi^{\mp}\Sigma^{\pm}$" Monte Carlo simulation. Red, blue and black plot indicates the $d(K^-, n)$"$\pi^-\Sigma^+$", the $d(K^-, n)$"$\pi^+\Sigma^-$" and average of these, respectively. Fitted 3rd polynomial function is plotted at same time.

Appendix C

$K^-d \to K^0nn$ events

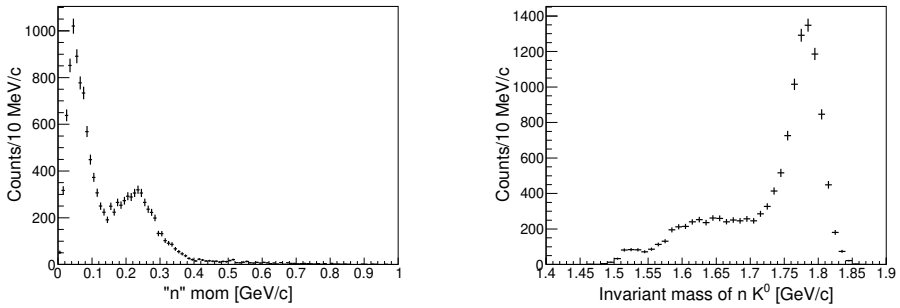

Figure C.1: Left figure indicates missing neutron momentum distribution in $d(K^-, nK^0)"n"$ events. Right figure indicates invariant mass of nK^0 in same event sample.

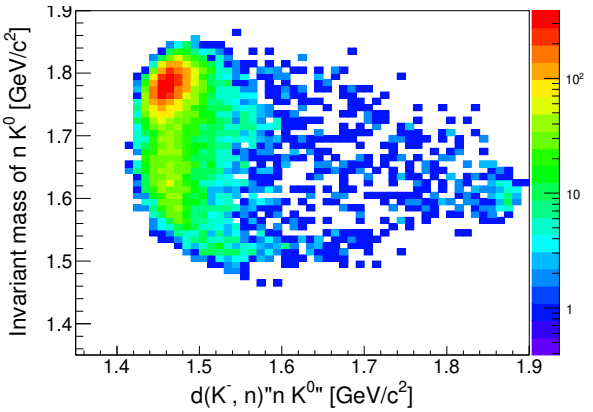

Figure C.2: This figure represents scatter plot of the $d(K^-, n)"nK^0"$ and invariant mass of the nK^0 which are detected particles.

In the $d(K^-, n)"nK^0"$ reaction, the missing neutron momentum disribu-

tion should be corresponding to fermi motion distribution. Invariant mass distribution of $n_{detected}K^0$ should also be distributed just below the kinematical threshold which is about $1.8GeV/c^2$ with $1GeV/c^2$ K^- beam. On the other hand, the missing neutron momentum distribution was observed high momentum component and the invariant mass of $n_{detected}K^0$ was observed widly distributed component in the data as FigC.1. Such widly distribution is not observed in the $d(K^-, n)"nK^0"$ distribution as FigC.2.

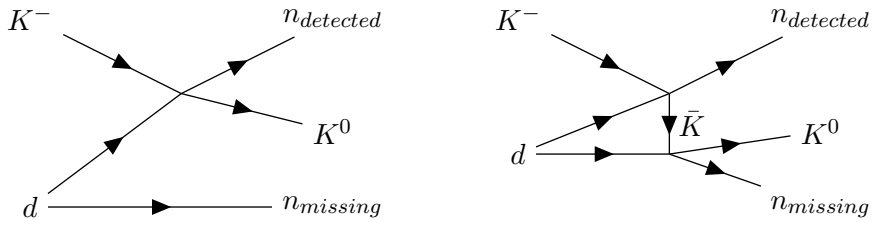

Figure C.3:

FigC.3 indicates feynmman daiagram of 1-step reaction and 2-step reaction of $K^-d \to K^0nn$ final state. $d(K^-, n)"nK^0"$ spectrum strongly reflects to 1-step $\bar{K}N$ scattering, on the other hand invariant mass of $n_{detected}K^0$ strongly reflects to interaction between recoiled $\bar{K}$ and residual nucleon. We simulated this reaction using following simply assamption. The 1-step reaction was simulated quasi-elastic scattering of $K^-p \to K^0n$ reaction and recoild K^0 rescattered with residual nucleon isotropically. In left figure of FigC.1, a bump structure around $\Lambda(1520)$ is seen. So, We also simulated $K^-n \to n_{forward}\Lambda(1520)$ reaction.
We perfom fitting for invariant mass spectra to estimate ratio of 2-step like reaction. In this fitting, strength of $\pi^{\mp}\Sigma^{\pm}$ was fixed and quasi-elastic (1-step) reaction, quasi-elastic with rescattering (2-step) reaction and $\Lambda(1520)$ production were free parameters. Fitting result indicats left figure of FigC.4. The momentum distribution of $n_{missing}$ and $d(K^-, n)"nK^0"$ were also shown in same figures.
According to this fitting, we obtained that the rations of 1-step, 2-step and $\Lambda(1520)$ production is 80%, 12% and 8% in $K^-d \to K^0nn$ final state.

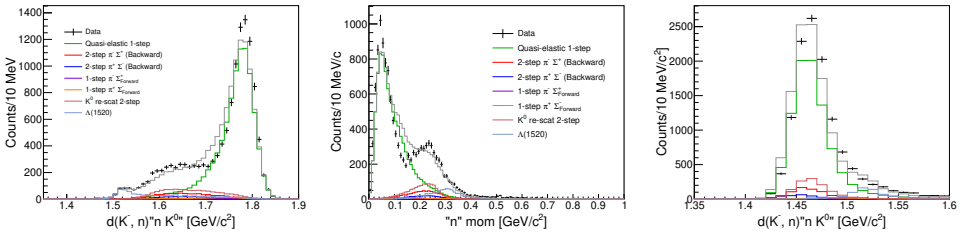

Figure C.4:

Appendix D

$d(K^-, p)$"$\pi^-\Lambda$"/"$\pi^-\Sigma^0$" mode

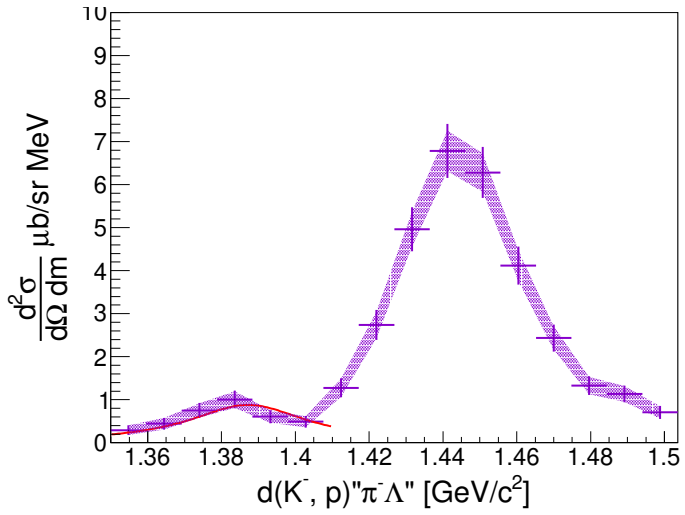

Figure D.1: This figure shows the obtained $d(K^-, p)$"$\pi^-\Lambda$" spectrum with $\Sigma(1385)^-$ fitting which indicats as red line.

We obtaine the cross section of the $d(K^-, p)$"$\pi^-\Lambda$" that is observed some structure around the $\Sigma(1385)$ region as shown in FigD.1. Although the $\Sigma(1305)$ whose isospin, spin and parity are $I(J^p) = 1(3/2^+)$ is P-wave, the pole due to the $\Sigma(1385)$ should appear 2-step effect that is constructive or destructive interferance term. A constructive contribution is clearly observed in the spectrum that was fitted with fixd mass and width whose values were adopted at $1387.2 MeV/c^2$ and $39.4 MeV/c^2$ respectively that is PDG [**?**] value.

The $\Sigma(1385)$ of the branching ratio of $\pi^-\Sigma^0$ against $\pi^-\Sigma^0$ is 0.135. The contribution to $\pi^-\Sigma^0$ mode of this branging ratio was ploted with our obtained spectrum in FigD.2 that is almost consistent.

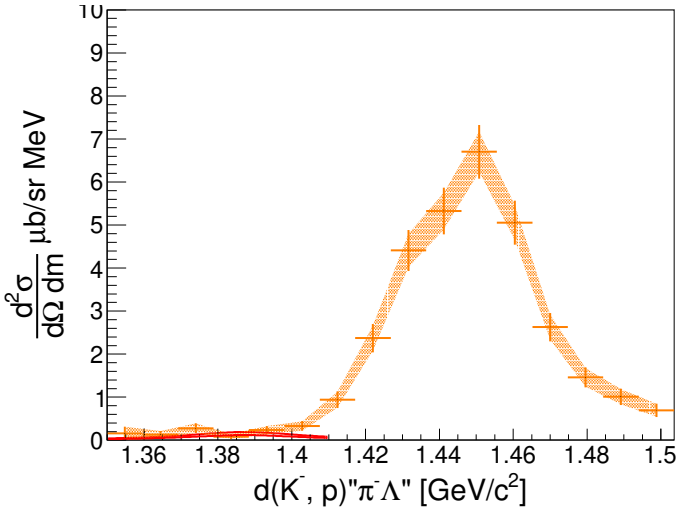

Figure D.2: This figure shows the obtained $d(K^-, p)$"$\pi^-\Sigma^0$" spectrum with $\Sigma(1385)^-$ contribution that was estimated from $\pi^-\Lambda$ mode.

Bibliography

[1] R. H. Dalitz and S. F. Tuan, Phys. Rev. Lett. 2 (1959).
"Possible Resonant State in Pion-Hyperon Scattering"

[2] M. H. Alston, L. W. Alvarez, P. Eberhard and M. L. Good,
Phys. Rev. Lett. 6, 698 (1961).
"Study of Resonances of the $\Sigma - \pi$ System"

[3] R. H. Dalitz, T. C. Wong and G. Rajasekaran,
Phys Rev. **153**, 1617 (1967)
"Model Calculation for the $Y^*(1405)$ Resonance State"

[4] R. J. Hemingway, Nucl Phys B **253**, 742 (1985).
"Production of $\Lambda(1405)$ in $K^- p$ Reactions at 4.2GeV/c"

[5] R. H. Dalitz and A. Deloff, J. Phys. G17, 281 (1991).
"The Shape and Parameters of the $\Lambda(1405)$ Resonance"

[6] A. D. Martin, Nucl. Phys. B **179**, 33 (1981).
"Kaon-Nucleon Parameters"

[7] J. D. Davies et el., Phys. Lett. B **83**, 55 (1979).
"Obserbation of Kaonic Hydrogen Atom X-rays"

[8] M. Izychi et el., Z. Phys. A **297**, 11 (1980).
"Results of the Search for K-series X-rays from Kaonic Hydrogen"

[9] H. Zhang et el., Phys. Rev. C **88**, 035204 (2013).
"Partial-wave analysis of $\bar{K}N$ scattering reactions"

[10] H. Zhang et el., Phys. Rev. C **88**, 035205 (2013).
"Multichannel parametrization of $\bar{K}N$ scattering amplitudes and extraction of resonance parameters"

[11] P. M. Bird et el., Nucl. Phys. A **404**, 482 (1983).
"Kaonic Hydrogen Atom X-rays"

[12] M. Iwasaki et el., Phys. Rev. Lett. **78**, 3067 (1997).
"Observation of Kaonic Hydrogen K_α X Rays"

[13] H. Noumi et al., Proposals for the 15th PAC meeting
"Spectroscopic study of hyperon resonances below $\bar{K}N$ threshold via the (K^-, n) reaction on Deuteron"

[14] M. Bazzi et el., Phys. Lett. B **704**, 113 (2011).
"A New Measuerment of Kaonic Hydrogen X-Rays"

[15] Y. Ikeda, T. Hyodo, and W. Weise, Nucl. Phys. A **881**, 98 (2012)
"Chiral SU(3) theory of antikaon–nucleon interactions with improved threshold constraints"

[16] T. Hyodo and U.-G. Meiβner, PDG Review, Tables and Plots, Section.83
"Pole Structure of the $\Lambda(1405)$ Region"

[17] T. Hashimoto et el., Phys. Rev. Lett. **128**, 112503 (2022).
"Measurements of Strong-Interaction Effects in Kaonic-Helium Isotopes at Sub-eV Precision with X-Ray Microcalorimeters"

[18] J. Zmeskal et el., J-PARC P57 Proposal
"Measurement of the Strong Interaction Induced Shift and Width of the 1s State of Kaonic Deuterium at J-PARC"

[19] G. P. Gopal et al., Nucl. Phys. B **119**, 362 (1977).
"Partial-wave analyses of KN two-body reactions between 1480 and 2170 MeV"

[20] N.KaiserP.B.Siegel and W.Weise, Nucl Phys A **594**, 325 (1995).
"Chiral Dynamics and the Low-Energy Kaon-Nucleon Interaction"

[21] D. Jido et el., Nucl. Phys. A **725**, 181 (2003).
"Chiral Dynamics of the Two $\Lambda(1405)$ States"

[22] Jonathan M. M. Hall et el, Phys. Rev. Lett. **114**, 132002 (2016).
"Lattice QCD Evidence that the $\Lambda(1405))$ Resonance is an Antikaon-Nucleon Molecule"

[23] H. Kamano et el., Phys. Rev. C **90**, 065202 (2014).
"Dynamical Coupled-Channels Model of K^-p Reactions: Determination ofPpartialWwaveAamplitudes"
Phys. Rev. C**92**, 025205 (2015).
"Dynamical Coupled-Channels Model of K^-p Reactions. II Extraction of Λ^* and Σ^* Hyperon Resonances"
Phys. ReV. C**95**, 044903(E) (2015).

[24] L. Roca and E. Oset, Phys. Rev. C **87**, 055201 (2013).
"$\Lambda(1405)$ poles obtained from $\pi^0\Sigma^0$ photoproduction data"

[25] S. X. Nakamura and D. Jido, Phys. Theor. Exp. Phys., **2014**, 023D01 (2014).
"Lambda (1405) photoproduction based on the chiral unitary model"

[26] J. Esmaili, Y. Akaishi, and T. Yamazaki, Phys. Lett. B **686**, 23 (2010)
"Experimental confirmation of the $\Lambda(1405)$ ansatz from resonant formation of a K^-p quasi-bound state in K^- absorption by ^{3}He and ^{4}He"

[27] M. Hassanvand et el., Phys. Rev. C **87**, 055202 (2013)
"Theoretical analysis of $\Lambda(1405) \to (\pi\Sigma)^0$ mass spectra produced in $p + p \to p + \Lambda(1405) + p$ reactions"

[28] J. Siebenson and L. Fabbietti, Phys. Rev. C **88**, 055201 (2013)
"Investigation of the $\Lambda(1405)$ line shape observed in pp collisions"

[29] M. Niiyama et el., Phys. Rev. C **78**, 035202 (2008).
"Photoproduction of $\Lambda(1405)$ and $\Sigma(1385)$ on the proton at $E_\gamma = 1.5$-2.4GeV/c"

[30] M. Niiyama et el., Phys. Rev. C **78**, 035202 (2008).
"Photoproduction of $\Lambda(1405)$ and $\Sigma(1385)$ on the proton at $E_\gamma = 1.5$-2.4GeV/c"

J. K. Ahn, Nucl. Phys. A **721**, 715c (2002).
"$\Lambda(1405)$ photoproduction at Spring-8/LEPS"

[31] K. Moria for the CLAS Collaboration,
Phys. Rev. C **87**, 035206 (2013).
"Measurement of the $\pi\Sigma$ photoproduction line shapes near the $\Lambda(1405)$"

[32] K. Moria for the CLAS Collaboration,
Phys. Rev. Lett. **112**, 082004 (2014).
"Spin and parity measurement of the $\Lambda(1405)$ baryon"

[33] J.C.Nacher et el., Phys. Lett. B **455**, 55 (1999).
"Photoproduction of the $\Lambda(1405)$ on the proton and nuclei"

[34] G. Agakishiev for the HADES Collaboration,
Phys. Rev C **87**, 025201 (2013).
"Baryonic Resonances to the $\bar{K}N$ threshold: The case of $\Lambda(1405)$ in pp collisions"

[35] A. Cieplý and J. Smejkal, Nucl. Phys. A **881**, 115 (2012).
"Chirally motivated $\bar{K}N$ amplitudes for in-medium applications"

[36] L.Fabbietti et el., Nucl. Phys. A **914**, 60 (2013).

[37] O. Braun et el., Nucl. Phys. B **129**, 1 (1977).
"New Information About the Kaon-Nucleon-Hyperon Coupling Constants $g(KN\Sigma(1197)), g(KN\Sigma(1385))$ and $g(KN\Lambda(1405))$"

[38] D. Jido, E. Oset and T. Sekihara, Eur. Phys. J. A **42**, 257 (2009).
"Kaonic Production of $\Lambda(1405)$ off deuteron target in chiral dynamics"

[39] K. Miyagawa, J. Haidenbauer, and H. Kamada Phys. Rev. C **97**, 055209 (2018)
"Faddev approach to the reaction $K - d \to \pi\Sigma n$ at $p_K = 1.0GeV/c$"

[40] S. Kawasaki et al., JPS Conf. Proc. **13**, 020018 (2017).
"Spectroscopic Experiment of $\Lambda(1405)$ via the In-flight $d(K^-, n)$n) Reaction at J-PARC K1BR.8"

[41] E. Oset, A. Ramos, and C. Bennhold, Phys. Lett. B **527**, 99 (2002); **530**, 260(E) (2002).
"Low lying $S = -1$ excited baryons and chiral symmetry"

[42] H. Zhang, et el., Phys. Rev. C **88**, 035204 (2013). "Partial-wave analysis of $\bar{K}N$ scattering reactions"

[43] S. Ohnishi et el, Phys. Rev. C **93**, 025207 (2016).
"Strcture of the $\Lambda(1405)$ and the $K^-d \to \pi\Sigma n$ reaction"

[44] H. Kamano et el., Phys. ReV. C**94**, 065205 (2016).
"Toward Establishing Low-Lying Λ and Σ Hyperon Resonances with the $\bar{K} + d \to \pi + Y + N$ Reaction"

[45] T. Hyodo and D. Jido, Prog. Part. Nucl. Phys. **67**, 55 (2012).
"The Nature of the $\Lambda(1405)$ Resonace in Chiral Dynamics"

[46] K. Agari et el, Prog. Theor. Exp. Phys., 02B009 (2012)

[47] K. Agari et el, Prog. Theor. Exp. Phys., 02B011 (2012)

[48] TRANSPORT http://linac96.web.cern.ch/Linac96/Proceedings/Thursday/THP72/Paper.pdf

[49] T. K. Ohska et al., Nuclear Science, IEEE Transactions on 33, 98 (1986).

[50] M. Shiozawa and et el., A new TKO system manager board for a dead-time-free data acquisition system, in 1994 IEEE Nuclear Science Symposium-NSS'94, pages 632–635, (1994)

[51] M. Iio et al., Nucl. Instrum. Methods Phys. Res., Sect. **A** 687, 1 (2012).

[52] S. Agostinelli et al., Nucl. Instrum. Methods Phys. Res., Sect. **A** 506, 250 (2003)
J. Allison et el., IEEE Transactions on Phys. Sci. 53, 207 (2006)
J.Allison et al., Nucl. Instrum. Methods Phys. Res., Sect. **A** 835, 186 (2016)

[53] K. Fuji, `https://www-jlc.kek.jp/subg/offl/lib/docs/helix_manip/node3.html` (1968).

[54] Opera Electromagnetic FEA Solution Software

[55] V. Flaminio et al., CERN-HARA-87-01, 121 (1983).

[56] M.Jones et el, Nucl. Phys. B **90**, 349 (1975)

[57] R. Barlow and C. Beeston, Comp. Phys. Comm. **77**, 219 (1993).

[58] A. Nappi, Comp. Phys. Comm. **180**, 269 (2009).

[59] M. jones, R. Levi, Setti, D. Merrill and R. D. Tripp, Phys. Rev. B**90**, 349 (1975).

[60] M. Bernheim and et. el., Nucl. Phys. A**365**, 349, (1981).

[61] R. Machleidt, Phys. Rev. C**63**, 024001 (2001).

[62] S. Agostinelli et al., Nuclear Instruments and Methods in Physics Research Section A: Accelerators, Spectrometers, Detectors and Associated Equipment **506**, 250 (2003).
J.Allison et el., Nuclear Instruments and Methods in Physics Research Section A: Accelerators, Spectrometers, Detectors and Associated Equipment **835**, 186 (2016).